Mi *et al.*
Protection and Control of Modern Power Systems (2022) 7:31
https://doi.org/10.1186/s41601-022-00250-1

Protection and Control of Modern Power Systems

ORIGINAL RESEARCH Open Access

Frequency control of a wind-diesel system based on hybrid energy storage

Yang Mi[1], Boyang Chen[1], Pengcheng Cai[1], Xingtang He[2], Ronghui Liu[1] and Xingwu Yang[1*]

Abstract

To improve the stability of a wind-diesel hybrid microgrid, a frequency control strategy is designed by using the hybrid energy storage system and the adjustable diesel generator with load frequency control (LFC). The objective of frequency control is to quickly respond to the disturbed system to reduce system frequency deviation and restore stability. By evaluating the area control error, the disturbance state of the system can be divided into four different areas by a corresponding control strategy for precise adjustments. For the diesel generator, an adaptive sliding mode (SM) algorithm is used to design LFC that can participate in frequency modulation. The frequency coordination control strategy proposed in this paper can realize the partition adjustment according to different resources, and ensure frequency stability. The proposed control strategy is verified by RTDS simulations in multiple scenarios.

Keywords: Wind-diesel microgrid, Hybrid energy storage, Load frequency control, Sliding mode adaptive algorithm

1 Introduction

For the wind-diesel based microgrid, the fluctuation of wind energy, random load and uncertain system parameters may cause large frequency deviations [1, 2]. With only diesel generator adjustment, it is difficult to assure the frequency stability because of its long response time. Thus, energy storage equipment is often installed to optimize the frequency control [3, 4].

Many optimization studies have been carried out on energy storage systems [5–12]. Based on a superconducting magnetic energy storage system, a frequency control method is proposed in [6] to reduce system frequency deviation. In [7], each doubly-fed induction generator wind turbine is equipped with an ultra-capacitor, and a two-layer constant power control scheme is proposed to control active power and regulate the grid frequency. In [8], superconducting magnetic energy storage is used to assist load frequency control (LFC) to smooth the frequency fluctuation, while in [9], the frequency stability is considered by using energy storage technology with an advanced control method. In order to improve the efficiency of the energy storage system, the hybrid energy storage system (HESS) with coordinated control strategy is applied to smooth the frequency deviation.

Energy storage devices may be an effective technology to smooth the frequency deviation, but large-scale energy storage can increase the cost of the microgrid. However, LFC can often be designed for a renewable power system to realize frequency control. In [13], an adaptive LFC is designed for a multi-area diesel power system to improve frequency stability, whereas in [14], a fuzzy PI LFC is constructed for the interconnected power system including wind energy. The sliding mode (SM) algorithm can also be used to design LFC because of its robust performance [15–19]. In [15], the SM method is used to design the vector control for the stability of a power system with high wind energy penetration, while in [16], an SM frequency control is proposed for an interconnected power system. SM LFC is also constructed to assure system frequency stability based on the disturbance observer [17, 18]. This can improve controller accuracy. In [19], a double SM controller is designed for an isolated microgrid

*Correspondence: yangxingwu@shiep.edu.cn

[1] School of Electric Power Engineering, ShangHai University of Electric Power, Shanghai 200090, China
Full list of author information is available at the end of the article

with renewable sources and the system frequency deviation can be effectively reduced.

In order to realize the partition adjustment of frequency when the system is disturbed, this paper introduces a new control strategy, one which combines LFC and Hess to quickly and accurately adjust the frequency of the wind power diesel power generation system. The main contributions of this paper can be summarized as follows:

(1) LFC is proposed to take part in the frequency adjustment on the source side. This uses an adaptive SM algorithm, so that the diesel output power can be controlled to optimize the frequency deviation.
(2) An HESS composed of battery and high energy density ultra-capacitor is used to improve the frequency stability making full use of the respective characteristics of different energy storage devices.
(3) In order to improve the accuracy of frequency regulation, the ACE signals are divided into four regions so that different power generation units can respond to the control signals according to different ACE regions.
(4) Different scenarios are designed to simulate the disturbance of the microgrid. RTDS simulation results show that the proposed new coordinated control strategy can effectively cope with the disturbance for the distributed source. At the same time, a research case is proposed for comparison to prove the strategies designed in this paper.

The rest of the paper is organized as follows. The wind-diesel microgrid model is introduced in Sect. 2. In Sect. 3, the frequency control strategy with the designed adaptive SM LFC and HESS is proposed, while Sect. 4 shows the simulation results in multiple scenarios. Finally, the summary is given in Sect. 5.

2 Model of wind-diesel microgrid

The wind-diesel hybrid microgrid is composed of wind power unit, diesel generator, ultra-capacitor unit, battery unit and load. Among them, the diesel generator is the main power source of the microgrid, the penetration ratio of the wind power is about 30%, and the rest of the power is borne by the energy storage. The topological structure of the system model is shown in Fig. 1.

From Fig. 1, it can be seen that the diesel generator and wind power generator are connected to the system bus. The control center can give different reference instructions for different working conditions according to the

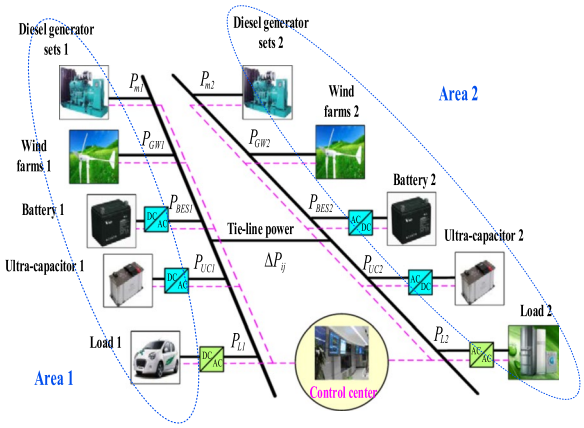

Fig. 1 Block diagram of wind-diesel micro-grid

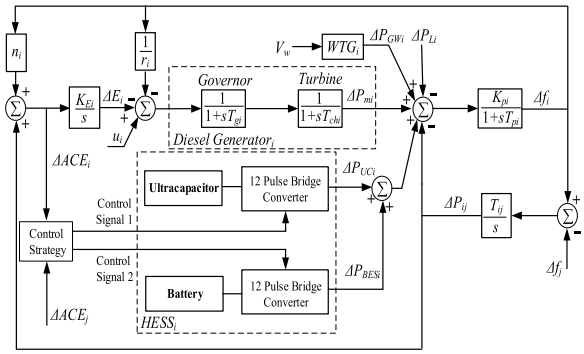

Fig. 2 The *i*th transfer function model of the wind-diesel microgrid

fluctuation of wind and load power. The active power balance equation of the *ith* area is given as:

$$P_{mi} + P_{GWi} + P_{BESi} + P_{UCi} - P_{ij} = P_{Li} \quad (1)$$

where $i = 1, 2$, $j = 1, 2$ and $i \neq j$. P_{mi} is the diesel generator output power, P_{GWi} is the wind turbine generator (WTG) output power, P_{BESi} is the charging or discharging power of BES, P_{UCi} is the ultra-capacitor charging or discharging power, ΔP_{ij} is the transmitted power of the tie-line, and P_{Li} is the area active load.

The detailed transfer function model of each area is shown in Fig. 2 [20].

From Fig. 2, it can be seen that the diesel generator model consists of a governor and turbine. The adaptive SM LFC control output $u_i(t)$ is designed for the governor of the diesel generator to regulate its output power. The controller can generate control signal 1 and control signal 2 by the ACE of different areas, which are then fed to the battery and capacitor for power regulation. The process of deriving the dynamic equation of the *ith* region is:

$$\begin{aligned}\Delta\dot{f}_i(t) = &-\frac{1}{T_{pi}}\Delta f_i(t) + \frac{K_{pi}}{T_{pi}}(\Delta P_{mi}(t) + \Delta P_{UCi}(t) + \Delta P_{BESi}(t) + \Delta P_{GWi}(t)) \\ &-\frac{K_{pi}}{T_{pi}}\left(\Delta P_{Li}(t) + \Delta P_{ij}(t)\right)\end{aligned} \tag{2}$$

$$\begin{aligned}\Delta\dot{P}_{mi}(t) &= -\frac{1}{T_{chi}}\Delta P_{mi}(t) + \frac{1}{T_{chi}}\Delta P_{vi}(t) \\ \Delta\dot{P}_{vi}(t) &= -\frac{1}{T_{gi}r_i}\Delta f_i(t) - \frac{1}{T_{gi}}\Delta P_{vi}(t) \ - \frac{1}{T_{gi}}\Delta E_i(t) + \frac{1}{T_{gi}}u_i(t)\end{aligned} \tag{3}$$

$$\Delta\dot{E}_i(t) = K_{Ei}n_i\Delta f_i(t) + K_{Ei}\Delta P_{ij}(t) \tag{4}$$

$$\Delta\dot{P}_{ij}(t) = T_{ij}[\Delta f_i(t) - \Delta f_j(t)] \tag{5}$$

where $\Delta f_i(t)$, $\Delta P_{mi}(t)$, $\Delta P_{vi}(t)$, $\Delta P_{Li}(t)$, and $\Delta P_{ij}(t)$ are, respectively, the change of frequency, adjustable generator output power, governor value position, load disturbance and the tie-line power. $\Delta E_i(t)$ and $u_i(t)$ are the integral control and control signal generated by the local LFC, respectively. T_{ij} is the interconnection gain between the i^{th} and j^{th} areas, T_{pi}, T_{chi} and T_{gi} are the time constants of the system, turbine and governor, respectively. K_{pi} and K_{Ei} are the respective gains of the system and integral control, r_i is the governor speed regulation coefficient, and n_i is the frequency bias factor.

2.1 Model of BES

In previous studies [21], the BES model is described as a first-order transfer function, but the model can be improved for better accuracy as in [22]. The main component of the BES is composed of parallel/series connected battery cells and the cascaded controllable bridge circuit connected to the $Y/\Delta - Y$ transformer. The equivalent circuit model of the BES is shown in Fig. 3.

From Fig. 3, the DC voltage of the battery V_{bt} before the power electronics inverter is given as:

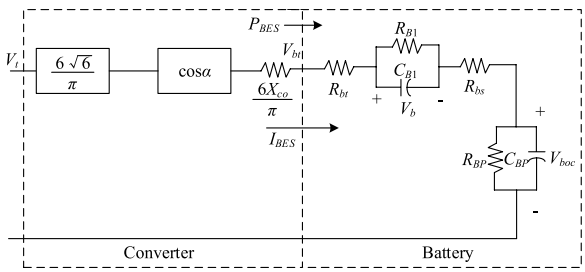

Fig. 3 The equivalent circuit model of BES

$$V_{bt} = \frac{3\sqrt{6}}{\pi}V_t(\cos\alpha_1^\circ + \cos\alpha_2^\circ) - \frac{6}{\pi}X_{co}I_{BES} \tag{6}$$

where V_t is the phase voltage in the AC side, α_i° is the firing delay angle of converter i, X_{co} is the commutating reactance which can be ignored because of its small value. Direct current I_{BES} flowing into the battery is given as:

$$I_{BES} = \frac{V_{bt} - V_{boc} - V_b}{R_{bt} + R_{bs}} \tag{7}$$

where V_{boc} is the open circuit voltage of the battery, V_b is the voltage across the R–C. This models the dynamic behavior of the battery. R_{bt} is the connecting resistance, and R_{bs} is the internal resistance.

Multiplying (7) and (8) yields the active power absorbed by the BES as [23]:

$$\Delta I_d = \frac{1}{1+sT_C}(K_{CA}ACE_i - K_{vd}\Delta V_d) \tag{8}$$

2.2 Model of ultra-capacitor

The ultra-capacitor model can often be represented by a parallel capacitor and resistor circuit [24, 25], and its mathematical model can be described as:

$$\Delta I_d = \frac{1}{1+sT_C}(K_{CA}ACE_i - K_{vd}\Delta V_d) \tag{9}$$

$$\Delta V_d = \frac{R_U}{1+sR_UC_U}\Delta I_d \tag{10}$$

$$\Delta P_{UC} = (V_{do} + \Delta V_d)\Delta I_d \tag{11}$$

where ΔV_d,ΔI_d and ΔP_{UC} are the variations of the ultra-capacitor voltage, current and output power, respectively. K_{CA} is the control gain, T_C is the time constant, and K_{vd} is the gain of the voltage feedback. C_U and R_U are the

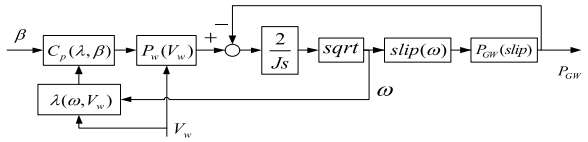

Fig. 4 Structure model of WTG

equivalent capacitance and resistance, respectively, while V_{do} is the initial capacitor voltage.

2.3 Model of WTG

The WTG configuration diagram is shown in Fig. 4, and its mechanical output power P_w is proportional to the cube of wind speed, expressed as [26, 27]:

$$P_w = \frac{C_p(\lambda,\beta)V_w^3\rho A_r}{2} \tag{12}$$

where V_w is the wind speed, ρ is the air density, A_r is the rotor cross section, $C_p(\lambda,\beta)$ is the power coefficient, β is the blade pitch angle, and $\lambda = A_r\omega/V_w$ is the tip speed ratio. The angular rotor speed ω is given by:

$$\omega^2 = \int \frac{2}{J}(P_w - P_{GW})dt \tag{13}$$

where J is the moment of inertia of the system.

If ω is faster or similar to the synchronous angular velocity of rotor ω_0, the WTG output power P_{GW} is given as [28]:

$$P_{GW} = \frac{-3V^2\varsigma(1+\tau)R_2}{(R_2-\varsigma R_1)^2+\varsigma^2(X_1+X_2)^2} \tag{14}$$

where V is the phase voltage, R_1 and R_2 are the stator and rotor resistances, respectively, X_1 and X_2 are the stator and rotor reactance, respectively, and the slip is $\varsigma = (\omega_0-\omega)/\omega_0$.

3 Frequency control strategy

3.1 Control principle

In the hybrid wind-diesel microgrid, the ACE is an important index to assure the stability of the system [29–31], and can be expressed as:

$$\Delta ACE_i = \Delta P_{ij} + n_i\Delta f_i \tag{15}$$

where n_i is the frequency deviation factor.

In order to improve the LFC accuracy, the ΔACE value can be divided into four control intervals according to the performance of different generators. ACE^N, ACE^A and ACE^E are the lower thresholds of normal regulation zone, alert regulation zone and emergency regulation zone, respectively. Based on those thresholds, four control zones can be defined as:

- $|\Delta ACE| \le ACE^N$ is the dead zone.
- $ACE^N < |\Delta ACE| \le ACE^A$ is the normal regulation zone.
- $ACE^A < |\Delta ACE| \le ACE^E$ is the alert regulation zone.
- $ACE^E < |\Delta ACE|$ is the emergency regulatory zone.

The system operational state is monitored by the dispatching center, which can quickly obtain the safe level of the system and the value of ΔACE to keep the balance between load and source.

3.1.1 The dead zone

In order to prevent unnecessary action of the governor system, a dead zone is set near the rated frequency. The tie-line power and frequency fluctuations in the dead zone are small, so a high-power density ultra-capacitor may be the best choice to resolve the small power fluctuations in the dead zone. The required power is given as:

$$E_{ACE}^D = \Delta ACE, \quad 0 < |\Delta ACE| \le ACE^N \tag{16}$$

where E_{ACE}^D is the total required power of the Dead Zone.

If E_{ACE}^D is positive, the ultra-capacitor absorbs excess power from the system, whereas the ultra-capacitor increases its output power when E_{ACE}^D is negative. Therefore, the response power of the ultra-capacitor in the dead zone is described as:

$$P_{uc}^D = \begin{cases} \min\left(|E_{ACE}^D|,\ P_{uc}^{dis-\max}\right), & -ACE^N \le \Delta ACE < 0 \\ \min\left(E_{ACE}^D,\ P_{uc}^{ch-\max}\right), & 0 < \Delta ACE \le ACE^N \end{cases} \tag{17}$$

where $P_{uc}^{dis-\max}$ and $P_{uc}^{dis-\max}$ are the ultra-capacitor's maximum allowable discharging and charging power, respectively.

3.1.2 The normal regulation zone

When a small disturbance occurs in the power system, it is usually considered that the frequency deviation and ACE are in the normal regulation area. Here, the adjustable generator with adaptive SM LFC is used to meet the frequency modulation requirements.

In the normal state, the total demand power is:

$$E_{ACE}^N = \Delta ACE\ ,\ \ ACE^N < |\Delta ACE| \le ACE^A \tag{18}$$

where E_{ACE}^N is total required power of the normal regulation zone.

The response power of the adjustable generator in the normal regulation zone is:

$$P_m^N = \begin{cases} \min\left(\left|E_{ACE}^N\right|, P_m^{in-\max}\right), & -ACE^A \le \Delta ACE < -ACE^N \\ \min\left(E_{ACE}^N, P_m^{de-\max}\right), & ACE^N < \Delta ACE \le ACE^A \end{cases} \tag{19}$$

where $P_m^{in-\max}$ and $P_m^{de-\max}$ are the allowable power of the total adjustable generators, and can be increased and decreased, respectively.

3.1.3 The alert regulation zone

In the alert regulation zone, the frequency deviation has exceeded the rated frequency range, and the ACE fluctuation is also large. Thus, HESS is used to reduce the frequency deviation, where the ultra-capacitor can provide high power input or output for a short period while the batteries with higher energy density can operate for longer periods of time. In addition, the adjustable generator with adaptive SM LFC can provide stable active power. Therefore, the respective characteristics of HESS and adjustable generator can be fully utilized to complement each other for the stable operation of the system.

The total required power used for frequency control is:

$$E_{ACE}^A = \Delta ACE,\ ACE^A < |\Delta ACE| \le ACE^E \tag{20}$$

where E_{ACE}^D is the total required power of the alert regulation zone.

The response power of the ultra-capacitor, BES and adjustable generator in the alert regulation zone is:

$$P_{uc}^A = \begin{cases} \min\left(\left|E_{ACE}^A\right|,\ P_{uc}^{dis-\max}\right), & -ACE^E \le \Delta ACE < -ACE^A \\ \min\left(E_{ACE}^A,\ P_{uc}^{ch-\max}\right), & ACE^A < \Delta ACE \le ACE^E \end{cases} \tag{21}$$

$$P_m^A = \begin{cases} \min\left(\left|E_{ACE}^A\right| - \left|P_{uc}^A\right|,\ P_m^{in-\max}\right), & -ACE^E \le \Delta ACE < -ACE^A \\ \min\left(E_{ACE}^A - P_{uc}^A,\ P_m^{de-\max}\right), & ACE^A < \Delta ACE \le ACE^E \end{cases} \tag{22}$$

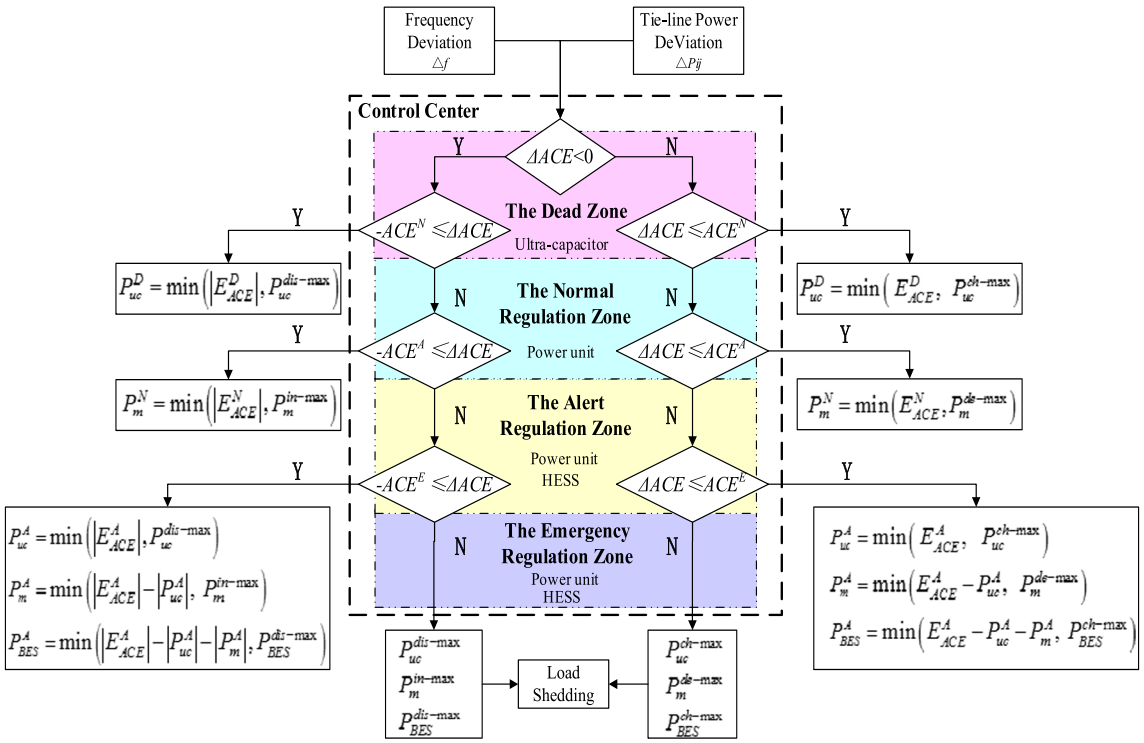

Fig. 5 The diagram of coordinated control strategy

$$P_{BES}^{A}=\begin{cases}\min\left(\left|E_{ACE}^{A}\right|-\left|P_{uc}^{A}\right|-\left|P_{m}^{A}\right|,\ P_{BES}^{dis-\max}\right), & -ACE^{E}\le\Delta ACE<-ACE^{A}\\ \min\left(E_{ACE}^{A}-P_{uc}^{A}-P_{m}^{A},\ P_{BES}^{ch-\max}\right), & ACE^{A}<\Delta ACE\le ACE^{E}\end{cases}\tag{23}$$

where $P_{BES}^{dis-\max}$ and $P_{BES}^{ch-\max}$ are the allowable maximum discharging and charging power of BES, respectively.

3.1.4 The emergency regulation zone

In the emergency regulation zone, a variety of frequency modulation devices are required to balance the active power. If the power equipment cannot significantly reduce frequency deviation, other measures need to be taken quickly, such as load shedding through power system dispatch.

From the above analysis, a diagram of the proposed control strategy is shown in Fig. 5.

3.2 The adaptive SM LFC design

Adaptive SM LFC is used to control the adjustable generator. The design process is described in the following sub-sections.

3.2.1 The switching surface design

The vector model of the system can be obtained from (2)-(6) as:

$$\dot{x}(t)=Ax(t)+Bu(t)+Fd(t)\tag{24}$$

where $x(t)$, A, B, F, $d(t)$ are given in the Appendix.

In an actual power system, the changes of load and output power can change the stable operation point of the system, so the normal state model in (25) can be refined as:

$$\dot{x}(t)=(A+\Delta A)x(t)+(B+\Delta B)u(t)+(F+\Delta F)d(t)\tag{25}$$

Defining $w(t)=\Delta Ax(t)+\Delta Bu(t)+(F+\Delta F)d(t)$ as the uncertainty, Eq. (26) can be expressed as:

$$\dot{x}(t)=Ax(t)+Bu(t)+w(t)\tag{26}$$

In order to design the controller, the following hypotheses are given [32–34]:

Hypothesis 1 (A,B) is totally controllable.

Hypothesis 2 $rank[B,w(t)]\neq rank[B]$

Hypothesis 3 the disturbance $w(t)$ is constrained, $\|w\|<\xi$, where $\|\ \|$ is matrix norm and ξ is a positive constant.

The following formula is chosen as the integral sliding mode surface:

$$\eta(t)=Cx(t)-\int C(A-BH)x(\tau)d\tau\tag{27}$$

where C and H are constant matrixes, matrix H has $\lambda(A-BH)<0$, while matrix C is selected to make CB nonsingular. According to stability analysis, when the system falls on the sliding mode plane, it is in a steady state.

3.2.2 The adaptive SM control laws design

Reaching law theory can enhance the dynamic performance of arrival phase, and the following equation is used to meet the condition:

$$\dot{\eta}(t)=-\hat{r}\eta(t)-\sigma\,\mathrm{sgn}\eta(t)\tag{28}$$

where σ is a non-negative constant, sgn$*$ is a symbolic function, and $\hat{r}$ is the estimation value. When multiple parameters are uncertain, for strong robustness of the controller, the parameter $\hat{r}$ satisfies the adaptive rule as:

$$\dot{\hat{r}}=a|\eta|\tag{29}$$

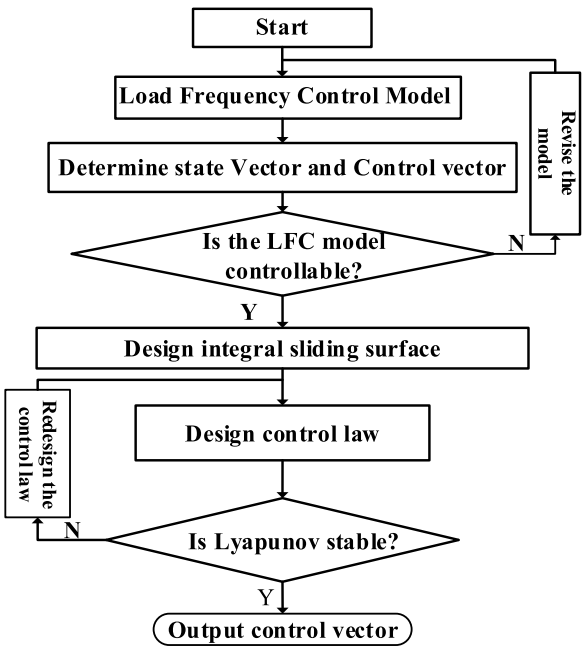

Fig. 6 flowchart of controller design

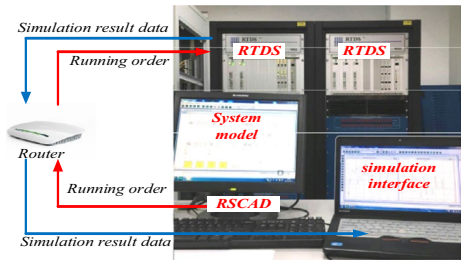

Fig. 7 The experimental setup based on RTDS

Table 1 The different scenarios

Operation scenario	Frequency control strategy	Generation unit		
		HESS	WTG	Diesel generator
Scenario 1	Quiet	Quiet	Quiet	Active
Scenario 2	Quiet	Quiet	Active	Active
Scenario 3	Quiet	Active	Active	Active
Scenario 4	Active	Active	Active	Active

where a is the adaptive positive constant.

From (29) and (30), there is:

$$\begin{aligned}\dot{\eta}(t) &= C\dot{x}(t) - C(A - BH)x(t)\\ &= CAx(t) + CBu(t) + Cw(t) - C(A - BH)x(t)\\ &= CBHx(t) + CBu(t) + Cw(t)\\ &= -\hat{r}\eta(t) - \sigma\,\mathrm{sgn}\eta(t)\end{aligned} \tag{30}$$

SM LFC is as follows:

$$u(t) = -Hx(t) - (CB)^{-1}[C\xi + \hat{r}\eta(t) + \sigma\,\mathrm{sgn}\eta(t)] \tag{31}$$

Since the system meets the condition of $\eta_i\dot{\eta}_i < 0$, the system is rendered stable using the designed controller. The flowchart of controller design is shown in Fig. 6.

4 RTDS simulation

Simulations for the microgrid are carried out in RTDS as shown in Fig. 7. The WTG, adjustable generator, HESS and load are simulated in the real-time simulator with 50 μs sampling time, whilst the coordinated control strategy is programmed in the microcontroller unit. The parameters of the model and control system are given in the Table 2. The input and output parameters in different cases are given in the Table 3.

In order to test the proposed control strategy, five cases are designed for different working conditions. Case 1 verifies the effectiveness of the proposed control strategy under step changes of wind output power and load. To reflect the different conditions of power system operation, cases 2 and 3 verify the superiority and general applicability of the proposed strategy under different power and load fluctuations. Because of the randomness and uncertainty of the actual system operation, the advantage of the proposed control strategy is further validated in case 4 under random wind power output and load disturbance. Finally, case 5 reflects the advantage of the proposed control strategy compared with other LFC algorithms in the literature [19].

Each case contains four operating scenarios, as:

- Scenario 1: the system disturbance is only the load fluctuation.
- Scenario 2: the wind power output is considered, and the system frequency is regulated by LFC.
- Scenario 3: HESS is added to the system, and each area responds to disturbance according to its local control.
- Scenario 4: HESS and SM LFC are coordinated to adjust frequency based on the proposed control strategy.

The different scenarios in the cases are shown in Table 1.

4.1 Case 1

In order to show the superiority of the proposed strategy, step load disturbance (0.3 p.u.) and step wind change (2 m/s) are added in two areas at 0 s and 90 s, respectively. Comparing scenarios 2, 3 and 4, the simulation results of frequency deviation and ACE deviation for the three different situations are shown in Fig. 8.

Figure 8a and b show the power change of scenario 3 and scenario 4, respectively. It can be seen that, under either load or wind speed fluctuation, the proposed coordinated control strategy results in better response, while scenario 2 with no HESS has the worst results among the three. Figure 8c shows that the response time of the system frequency of scenario 4 when the step load is added to the system is only 1.4 s, compared to more than 10 s for the other two scenarios. Therefore, the proposed coordinated control strategy can stabilize the frequency fluctuation, enhance the system adjustment speed and make the system more stable.

4.2 Case 2

Some emergencies may occur during actual operation of the microgrid, such as the shutdown of wind turbines. In order to simulate such uncertainty, case 2 is used to test this abnormal operational state. A step wind speed (2 m/s) is defined at 0 s, such that the system is in an

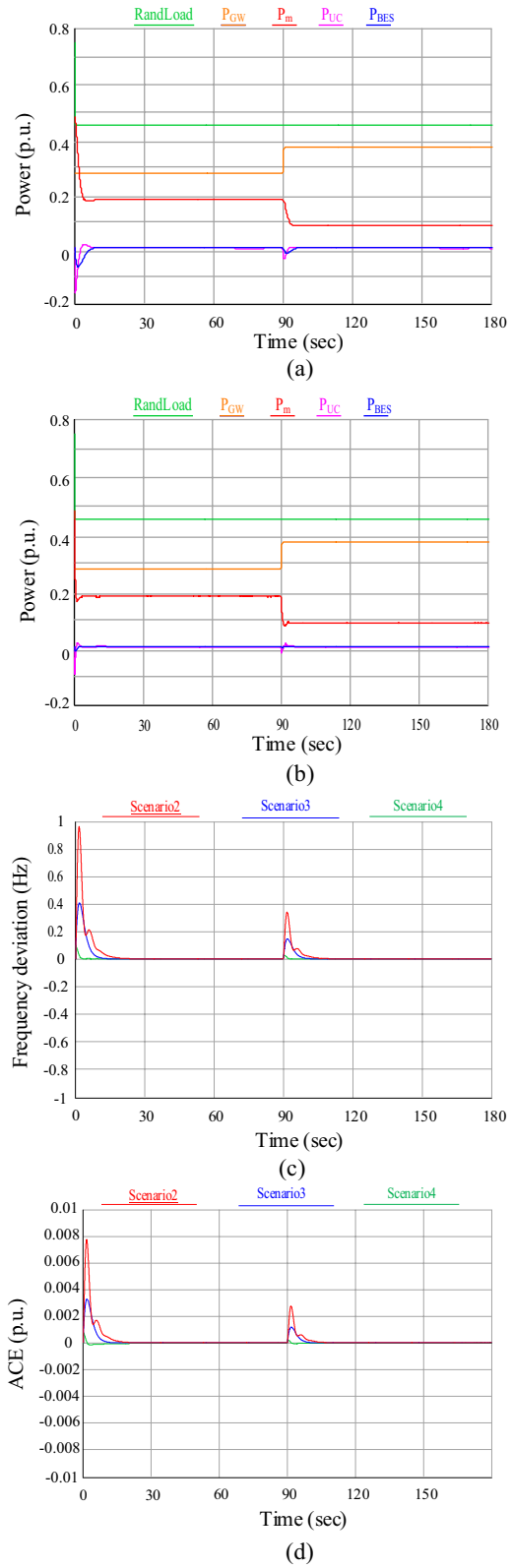

Fig. 8 Simulation results under step loads and wind speed, **a** power flow of scenario 3, **b** power flow of scenario 4, **c** system frequency deviation, **d** ACE deviation of area one

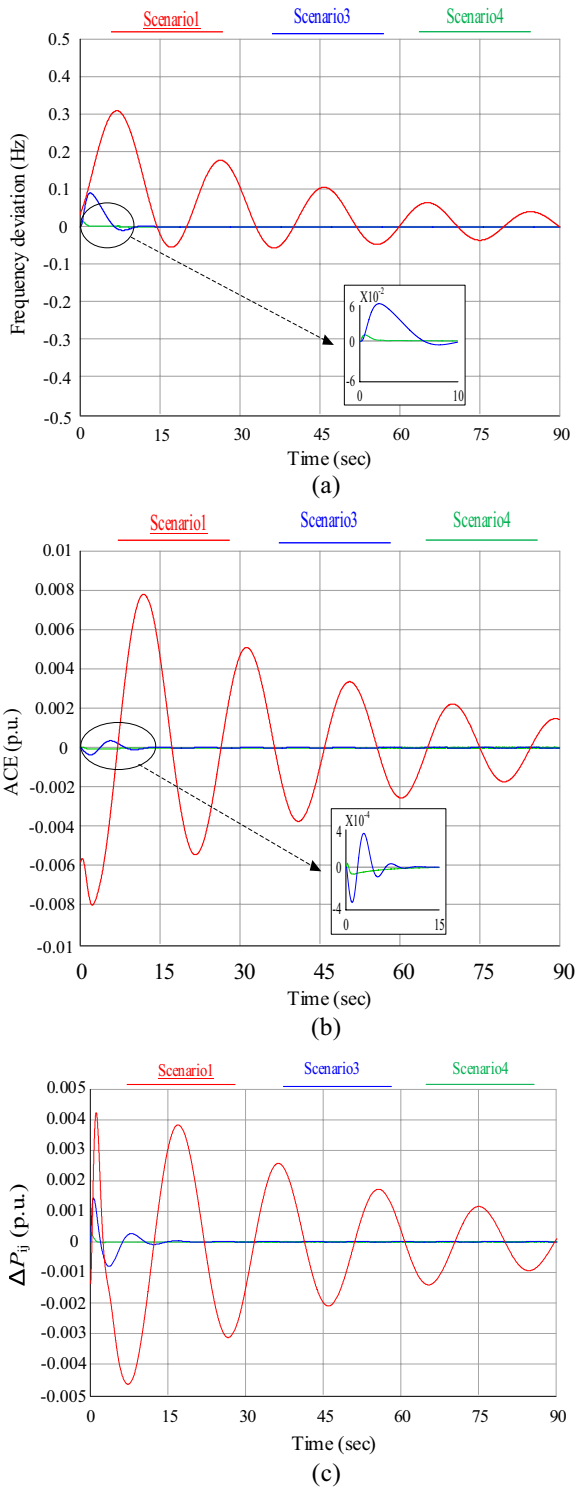

Fig. 9 Simulation results under step change of wind speed, **a** system frequency deviation, **b** ACE deviation of area one, **c** power deviation of tie-line

abnormal operation state and ΔACE is in the emergency regulation zone. Scenarios 1, 3 and 4 are tested and the simulation results of the area 1 frequency deviation, ACE deviation and the power deviation of the tie-line are shown in Figs. 9a–c, respectively.

As can be seen from Fig. 9a, the proposed control strategy makes frequency response faster and frequency deviation smaller. In addition, HESS is used to avoid frequency oscillation and make the system more stable. With different situations running in different zones, Fig. 9b shows that the maximum ACE deviation of scenario 4 is 4×10^{-5} p.u., and the system operates in the normal regulation zone. In contrast, the maximum ACE deviation of scenario 3 is 3.5×10^{-4} p.u., and the system operates in the alert regulation zone. However, the maximum ACE deviation of scenario 1 has exceeded the threshold of the emergency regulation zone, and the operation of the system is unstable. From Fig. 9c, ΔP_{ij} of scenario 1 is the largest, although the attenuation of the oscillation is presented, the system is still not stable after 90 s. In contrast, scenario 4 with coordinated control strategy makes the system stable within 1.5 s, and ΔP_{ij} deviation is also reduced.

4.3 Case 3

The load side disturbance in case 3 is used to simulate the uncertainty, and step load disturbances (0.05 p.u.) and (0.1 p.u.) are added to the two different areas, respectively. Scenarios 2, 3 and 4 are tested and the simulation results of the area 1 frequency deviation, ACE deviation and the power deviation of the tie-line are shown in Figs. 10a–c, respectively.

Figure 10 shows that the frequency deviation of scenario 4 is about 0.03 Hz, ACE deviation is about 2.62×10^{-4} p.u. and ΔP_{ij} is 2.1×10^{-4} p.u.. The frequency deviation, ACE deviation and ΔP_{ij} of scenario 3 are 0.11 Hz, 1.25×10^{-3} p.u., and 6.76×10^{-4} p.u., respectively. In scenario 2 without HESS and coordination control strategy, the frequency deviation, ACE deviation and ΔP_{ij} are beyond the normal ranges. Similarly, with the same conclusion as case 2, the proposed coordinated control strategy not only improves the system response speed, but also decreases the frequency deviation, so that the system can run stably in the normal zone.

4.4 Case 4

In case 4, random wind speed and load are considered. The balance state is broken, and ΔACE is in the alert regulation zone. Scenarios 2, 3 and 4 are tested. Figure 11 shows the power output of each generator and the consumption of the load in scenario 4. All three scenarios are simulated based on the same random load and WTG output power shown in Fig. 11.

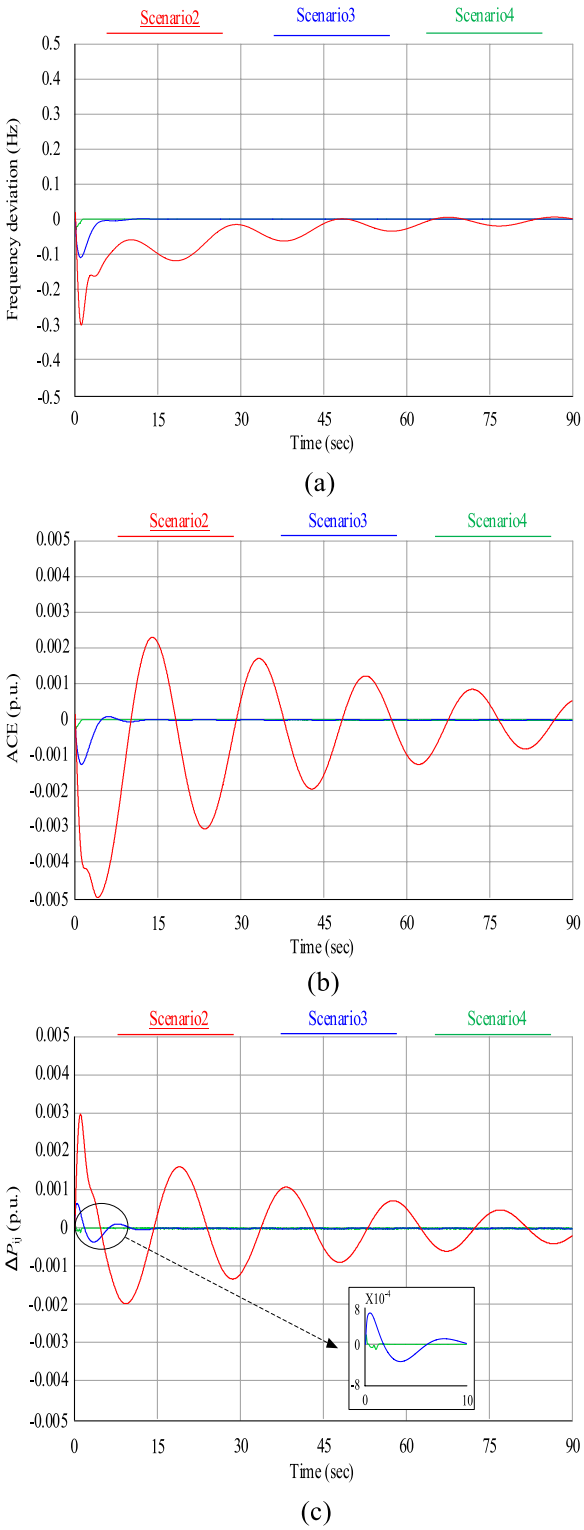

Fig. 10 Simulation results under step load, **a** system frequency deviation, **b** ACE deviation of area one, **c** power deviation of tie-line

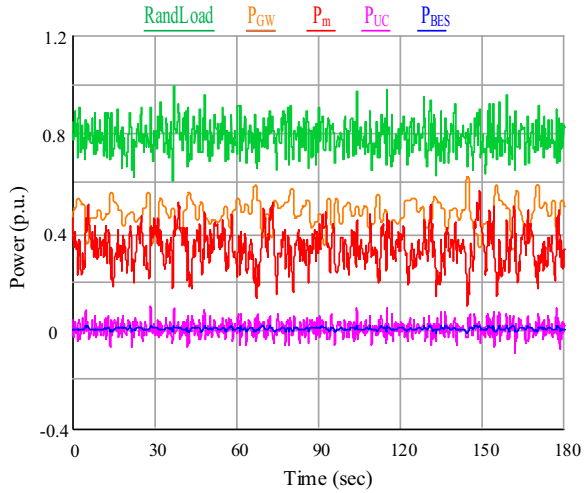

Fig. 11 Power flow of the system in scenario 4

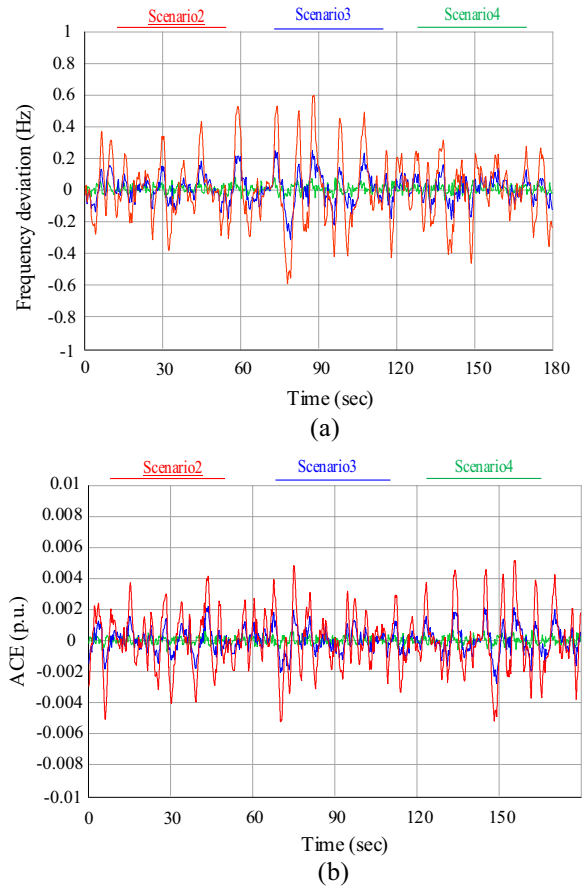

Fig. 12 Simulation results under random loads and wind speed, **a** system frequency deviation, **b** ACE deviation of area one

From Fig. 11, the system power fluctuations are quickly compensated by power generation units through the proposed control strategy. Simulation results of the frequency deviation and ACE deviation for the three different situations are shown in Fig. 12.

From the RTDS results in Fig. 12a, the maximum frequency deviation Δf_1 with scenario 4 is 0.08 Hz, while it is 0.34 Hz in scenario 3 and 0.56 Hz in scenario 2. Under the proposed control strategy, frequency deviation is within the range of 0.1 Hz. The response with the propose strategy also has smaller overshoot than the other two situations. Without HESS, the system frequency deviation is more than 0.5 Hz and the stability of the power system is

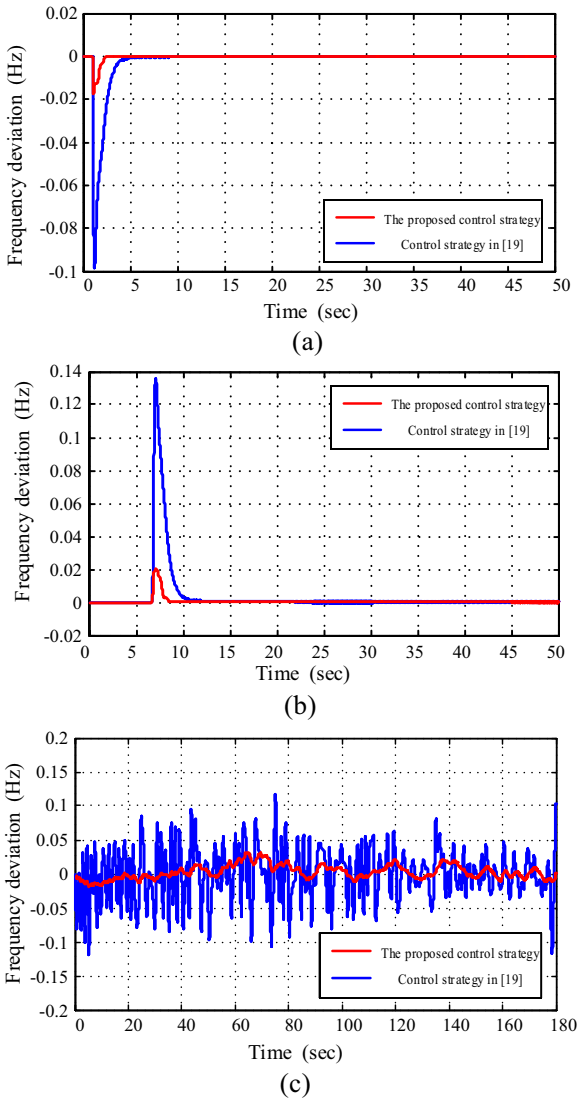

Fig. 13 Simulation results to verify the control strategy, **a** frequency deviation under the step load fluctuation, **b** frequency deviation under the step wind speed, **c** frequency deviation under the random power fluctuation

poor. Similarly, under the proposed control strategy, the ACE deviation is much smaller than the other two scenarios, and the system runs steadily in the normal zone. Without HESS, the ACE deviation has exceeded the threshold of the emergency regulation zone. This can easily put the system into the emergency state. Although the simulation results of scenario 3 are better than those of scenario 2, with HESS but without the proposed coordinated control strategy, the system still operates in the alert regulation zone. Therefore, the ultra-capacitor and BES must respond quickly and provide strong power input within a short time. After that, the adjustable generator regulates its output power under the adaptive SM LFC. Thus, the combination of HESS and adjustable generator can effectively improve the system frequency quality.

4.5 Case 5

In order to verify the superiority of the designed control strategy, we compare with the LFC algorithm proposed in [19]. As shown in Fig. 13a, the system frequency can be controlled under the step load fluctuation (0.05 p.u.) by using two control methods. Then, the step wind speed (15 m/s) is used to verify the control strategy in Fig. 13b. Finally, the system operates under the random load fluctuation and random WTG output power conditions as in Fig. 13c.

It can be seen from Fig. 13a that, with step load fluctuation, the frequency deviation of the existing LFC algorithm [19] is about 0.1 Hz and the response time is more than 5 s, while with the control method proposed in this paper they are reduced to 0.017 Hz and 2.21 s, respectively. Figure 13b shows that the system frequency deviation with the designed control strategy has smaller overshoot than that with the existing LFC algorithm [19] under the same source disturbance. It can also be seen from Fig. 13c that under the condition of random load fluctuation and random WTG output power, the frequency deviation with the existing frequency control algorithm is 0.127 Hz, compared to 0.048 Hz with the

Table 2 The part model parameters and control system parameters

The parameters of adjustable generator model			
Parameter	**Value**	**Parameter**	**Value**
frate (Hz)	50	K_{pi} (Hz/MW)	1
T_{pi} (sec)	10	r_i (Hz/MW)	0.05
T_{chi} (sec)	0.3	n_i (MW/Hz)	0.425
T_{gi} (sec)	0.2	T_{ij} (MW/Hz)	0.545
K_{Ei} (1/s)	1	PG-capacity (kW)	280
The parameters of HESS model			
Parameter	Value	Parameter	Value
R_{bs} (Ω)	0.013	R_{bt} (Ω)	0.0167
α_1°	15	α_2°	25
X_{CO} (Ω)	0.02744	E_{d0} (kV)	2
K_{CA} (kA/unitMW)	70	K_{vd} (kA/kV)	0.1
T_C (s)	0.05	R_U (Ω)	100
C_U (F)	1	PBES-capacity (kW)	100
PUC-capacity (kW)	80		
the parameters of WTG model			
Parameter	Value	Parameter	Value
A_r (m)	14	*J* (kg*m2)	62,993
ρ (kg*m3)	1.225	*V* (V)	230.94
R_1 (Ω)	0.00397	R_2 (Ω)	0.00443
X_1 (Ω)	0.00376	X_2 (Ω)	0.0534
P_{GW} (kW)	120		
Response thresholds of the proposed control strategy			
Parameter (p.u.)	Value (%)	Parameter (p.u.)	Value (%)
ACE^N	0.12	ACE^A	0.3
ACE^E	0.5		

Table 3 The input and output parameters in different cases

Operation case	**Case1**	**Case 2**	**Case 3**	**Case 4**	**Case 5**
Step load disturbance	0.3p.u				
(t = 0 s)	–	0.1p.u			
(t = 0 s)/ 0.05p.u					
(t = 0 s)	Random	0.05p.u			
(t = 0 s)					
Step wind disturbance	2 m/s				
(t = 90 s)	2 m/s				
(t = 0 s)	–	Random	15 m/s		
(t = 7 s)					
Maximum frequency deviation (Hz)	0.121	0.017	0.030	0.082	0.025
Maximum stability					
Recovery time(s)	2.21	0.90	1.63	–	1.51

proposed control method in this paper. When the system frequency fluctuates within 0.5 Hz, the system can maintain a stable state. Therefore, it can be concluded that the method proposed in this paper not only smooths out disturbances faster than the existing algorithm, but also controls the frequency deviation within a smaller range to ensure the stability of the system.

5 Conclusion

In this paper, based on HESS and an adjustable generator with adaptive SM LFC, a frequency control strategy for a wind-diesel microgrid is proposed. According to different ACE signals, the proposed control strategy can provide a targeted control strategy to achieve partition control. Five cases are designed for analysis and each case contains 4 different scenarios. The RTDS simulation results show that, under random disturbances in the system including source side and load side fluctuations, the proposed coordinated control strategy not only improves the response speed, but also reduces the frequency deviation, when compared to other existing methods.

Appendix

The specific contents of each matrix in (25) are as follows.

$$x(t) = \left[\, \Delta f_1 \Delta P_{m1} \Delta P_{v1} \Delta E_1 \Delta P_{12} \Delta f_2 \Delta P_{m2} \Delta P_{v2} \Delta E_2 \,\right]^T,$$
$$u = \left[\, u_1 \;\; u_2 \,\right]^T,$$

$$A = \begin{bmatrix} \frac{-1}{T_{p1}} & \frac{K_{p1}}{T_{p1}} & 0 & 0 & \frac{-K_{p1}}{T_{p1}} & 0 & 0 & 0 \\ 0 & \frac{-1}{T_{ch1}} & \frac{1}{T_{ch1}} & 0 & 0 & 0 & 0 & 0 \\ \frac{-1}{r_1 T_{g1}} & 0 & \frac{-1}{T_{g1}} & \frac{1}{T_{g1}} & 0 & 0 & 0 & 0 \\ K_{E1} n_1 & 0 & 0 & 0 & 1 & 0 & 0 & 0 \\ T_{12} & 0 & 0 & 0 & -T_{12} & 0 & 0 & 0 \\ 0 & 0 & 0 & \frac{K_{p2}}{T_{p2}} & \frac{-1}{T_{p2}} & \frac{K_{p2}}{T_{p2}} & 0 & 0 \\ 0 & 0 & 0 & 0 & 0 & \frac{-1}{T_{ch2}} & \frac{1}{T_{ch2}} & 0 \\ 0 & 0 & 0 & 0 & \frac{-1}{r_2 T_{g2}} & 0 & \frac{-1}{T_{g2}} & \frac{1}{T_{g2}} \\ 0 & 0 & 0 & 0 & -1 & K_{E2} n_2 & 0 & 0 \end{bmatrix}, \quad B = \begin{bmatrix} 0 & 0 \\ 0 & 0 \\ \frac{1}{T_{g1}} & 0 \\ 0 & 0 \\ 0 & 0 \\ 0 & 0 \\ 0 & 0 \\ 0 & \frac{1}{T_{g2}} \\ 0 & 0 \end{bmatrix}$$

$$F = \begin{bmatrix} \frac{-K_{p1}}{T_{p1}} & 0 & 0 & 0 & 0 & 0 & 0 & 0 \\ 0 & 0 & 0 & 0 & 0 & \frac{-K_{p2}}{T_{p2}} & 0 & 0 & 0 \end{bmatrix}$$

$$d(t) = \begin{bmatrix} \Delta P_{GW1} + \Delta P_{BES1} + \Delta P_{UC1} - \Delta P_{L1} \\ \Delta P_{GW2} + \Delta P_{BES2} + \Delta P_{UC2} - \Delta P_{L2} \end{bmatrix}$$

The part model parameters of wind-diesel hybrid microgrid and control system parameters are shown in Tables 2 and 3.

Abbreviations

HESS: Hybrid energy storage system; ACE: Area control error; LFC: Load frequency control; SM: Sliding mode; RTDS: Real-time digital simulation platform; WTG: Wind turbine generator; GTO: Gate turnoff thyristors; BES: Battery energy storage.

List of symbols

P_{mi}: Diesel generator output power; P_{GWi}: Wind turbine generator (WTG) output power; P_{BESi}: Charge or discharge power of BES; P_{UCi}: Ultra-capacitor charge or discharge power; ΔP_{ij}: Transmission power of tie-line; P_{Li}: Area active load; $u_i(t)$: Control signal generated by local LFC; $\Delta P_{Li}(t)$: Load disturbance; T_{ij}: Interconnection gain between *ith* area and *jth* area; T_{pi}: Time constants of system; T_{chi}: Time constants of turbine; T_{gi}: Time constants of governor; K_{pi}: Gain of system; K_{Ei}: Gain of integral control.

Acknowledgements

Not applicable.

Author's information

Yang Mi (1976-), female, Ph.D. and Professor, the main research direction is microgrid control, stable operation and control of power system. Boyang Chen, (1998-), male, postgraduate, Major in Optimal operation and control of microgrid. Pengcheng Cai, (1991-), male, postgraduate, the main research direction is renewable energy access to microgrid. Xingtang He, (1994-), male, postgraduate, the main research direction is artificial intelligence control technology to microgrid. Ronghui Liu (1975-), female, Ph.D. and Professor, the main research direction is Automatic control. Xingwu Yang, (1981-), male, Ph.D. and Professor, the main research direction is Power system reactive power compensation and harmonic suppression technology, wind power and solar grid connection control.

Author contributions

All authors contributed to the research concept. CBY modelled the system, designed the algorithm of control strategy, and wrote a paper. MY and FY put forward the initial concept and gave technical guidance in the whole process. CPC and HXT check the data and experimental results, and demonstrate the strategy proposed in the paper. L contributed to the revision and typesetting of the manuscript. All authors read and approved the final manuscript.

Funding

The author(s) disclosed receipt of the following financial support for the research, authorship, and/or publication of this article: This work was supported in part by the National Natural Science Foundation of China (no. 61873159) and Shanghai Municipal Natural Science Foundation (22ZR1425500).

Availability of data and materials

Please contact author for data and material request.

Declarations

Competing interests

The authors declare that they have no known competing financial interests or personal relationships that could have appeared to influence the work reported in this paper.

Author details

[1]School of Electric Power Engineering, ShangHai University of Electric Power, Shanghai 200090, China. [2]School of Electric Power Engineering, Tianjin University, Tianjin 300072, China.

Received: 23 November 2021 Accepted: 15 July 2022
Published online: 11 August 2022

References

1. Murty, V. V. S. N., & Kumar, A. (2022). Retraction note: Multi-objective energy management in microgrids with hybrid energy sources and

battery energy storage systems. *Protection and Control of Modern Power Systems, 7*, 11.
2. Zhang, S., Mishra, Y., & Shahidehpour, M. (2016). Fuzzy-logic based frequency controller for wind farms augmented with energy storage systems. *IEEE Transactions on Power Systems, 31*(2), 1595–1603.
3. Krishnan, V., Das, T., & McCalley, J. D. (2014). Impact of short-term storage on frequency response under increasing wind penetration. *Journal of Power Sources, 257*, 111–110.
4. Tang, Y., Bai, Y., Huang, C., et al. (2015). Linear active disturbance rejection-based load frequency control concerning high penetration of wind energy. *Energy Conversion and Management, 95*, 259–271.
5. Huang, K., Li, Y., Zhang, X., et al. (2021). Research on power control strategy of household-level electric power router based on hybrid energy storage droop control. *Prot Control Mod Power Syst, 6*, 13.
6. Magdy, G., Bakeer, A., & Alhasheem, M. (2021). Superconducting energy storage technology-based synthetic inertia system control to enhance frequency dynamic performance in microgrids with high renewable penetration. *Prot Control Mod Power Syst, 6*, 36.
7. Qu, L., & Qiao, W. (2011). Constant power control of DFIG wind turbines with super capacitor energy storage. *IEEE Transactions on Industry Applications, 47*(1), 359–367.
8. Magdy, G., Shabib, G., Elbaset, A. A., et al. (2018). Optimized coordinated control of LFC and SMES to enhance frequency stability of a real multi-source power system considering high renewable energy penetration. *Prot Control Mod Power Syst, 3*, 39.
9. Attya, A. B., Domínguez-García, J. L., Bianchi, F. D., et al. (2018). Enhancing frequency stability by integrating non-conventional power sources through multi-terminal HVDC grid. *International Journal of Electrical Power and Energy Systems., 95*, 128–136.
10. Chen, H., Xiong, R., Lin, C., & Shen, W. (2021). Model predictive control based real-time energy management for hybrid energy storage system. *CSEE Journal of Power and Energy Systems, 7*(4), 862–874.
11. Lu Y, Xu J, Zhao Y, Ye P, H. Li, "Optimal control of wind power hybrid energy storage system," 2017 First International Conference on Electronics Instrumentation & Information Systems (EIIS), Harbin, 2017, pp. 1–5.
12. Jeon J. H., Kim J. Y., Kim S. K., et al., "Unified compensation control of a hybrid energy storage system for enhancing power quality and operation efficiency in a diesel and wind-turbine based stand-alone microgrid,". In: 2012 3rd IEEE International Symposium on Power Electronics for Distributed Generation Systems, 2012, pp. 264–270.
13. Zribi, M., Al-Rashed, M., & Alrifai, M. (2005). Adaptive decentralized load frequency control of multi-area power systems. *International Journal of Electrical Power and Energy Systems, 27*(8), 575–583.
14. Zhou H., Fu Y., Cong R., "Fuzzy-based load frequency controller for interconnected power system with wind power integration," In: 2014 IEEE 27th Canadian Conference on Electrical and Computer Engineering, 2014, pp. 1–6.
15. Ayyarao, T. S. L. V. (2019). Modified vector controlled DFIG wind energy system based on barrier function adaptive sliding mode control. *Protection and Control of Modern Power Systems, 4*, 4.
16. Kumar, A., Anwar, M. N., & Kumar, S. (2021). Sliding mode controller design for frequency regulation in an interconnected power system. *Protection and Control of Modern Power Systems, 6*, 6.
17. Mi, Y., Fu, Y., Wang, C., et al. (2013). Decentralized sliding mode load frequency control for multi-area power systems. *IEEE Transactions on Power Systems, 28*(4), 4301–4309.
18. Mi, Y., & Wang, C. (2013). Frequency optimization control for isolated photovoltaic-diesel hybrid microgrid based on load estimation. *Proceedings of the Chinese Society for Electrical Engineering, 33*(34), 115–121.
19. Wang, C., Mi, Y., Fu, Y., et al. (2018). Frequency Control of an Isolated Micro-Grid Using Double Sliding Mode Controllers and Disturbance Observer. *IEEE Transactions on Smart Grid Transactions on Smart Grid, 9*, 923–930.
20. Wang, Y., Zhou, R., & Wen, C. (1993). Robust load-frequency controller design for power systems. *IEE Proceedings C Generation, Transmission and Distribution, 140*(1), 11. https://doi.org/10.1049/ip-c.1993.0003
21. Y. Lu, J. Xu, Y. Zhao, P. Ye and H. Li, "Optimal control of wind power hybrid energy storage system," 2017 First International Conference on Electronics Instrumentation & Information Systems (EIIS), Harbin, 2017, pp. 1–5
22. Aditya, S. K., & Das, D. (2001). Battery energy storage for load frequency control of an interconnected power system. *Electric Power System Research, 58*(3), 179–185.
23. Kimbark, E. W. (1971). *Direct Current Transmission* (Vol. 1, pp. 67–69). Wiley.
24. J. Gholinezhad, M. R. Safari and T. R. Noroozian, "SMES and CES controllers design for load frequency stabilization in two-area interconnected system," 2011 19th Iranian Conference on Electrical Engineering, Tehran, 2011, pp. 1–1.
25. Abraham, R. J., Das, D., & Patra, A. (2005). Effect of capacitive energy storage on automatic generation control. *International Power Engineering Conference, 2*, 1070–1074.
26. Sakamoto, R., Senjyu, T., Kaneko, T., et al. (2008). Output power leveling of wind turbine generator by pitch angle control using H ∞, control. *Electrical Engineering in Japan, 162*(4), 17–24.
27. Uehara, A., Senjyu, T., Yona, A., et al. (2010). A frequency control method by wind farm and battery using load estimation in isolated power system. *International Journal of Emerging Electric Power System, 11*(2), 1–20.
28. Senjyu, T., Sakamoto, R., Urasaki, N., et al. (2006). Output power leveling of wind turbine generator for all operating regions by pitch angle control. *IEEE Transactions on Energy Conversion, 21*(2), 467–475.
29. Kundur P. Power System Stability and Control. New York, USA: McGraw-Hill, pp 606–607, 1994.
30. Kothari, M. L., Nanda, J., Kothari, D. P., & Das, D. (1989). Discrete-mode automatic generation control of a two-area reheat thermal system with new area control error. *IEEE Transactions on Power Systems, 4*(2), 730–738.
31. Polajer, B., Petrun, M., & Ritonja, J. (2018). Adaptation of load-frequency-control target values based on the covariances between area-control errors. *IEEE Transactions on Power Systems, 33*(6), 5865–5874.
32. Gao, W., Wang, Y., & Homaifa, A. (1995). Discrete-time variable structure control systems. *IEEE Transactions on Industrial Electronics, 42*(2), 117–122.
33. Yan, X. G., Edwards, C., Spurgeon, S. K., et al. (2004). Decentralised sliding-mode control for multimachine power system using only output information. *IET Control Theory and Applications, 151*(5), 627–635.
34. Yan, X. G., Spurgeon, S. K., & Edwards, C. (2012). Global decentralised static output feedback sliding mode control for interconnected time-delay systems. *IET Control Theory and Applications, 6*(2), 192–202.